Flow in Driven Cavities with a Free Surface

A study of the flow of viscous liquids contained in an open cavity driven by a moving wall has been undertaken as a first step toward understanding interphase heat and mass transport in polymer processing equipment where rolling pools of liquid are generated. Solutions to the equations of motion for creeping flow in cavities of different aspect ratios were obtained using a finite-differences technique for circumstances when the wall moves in the same direction as the gravitational field.

Experimental studies of the flow patterns in cavities of various aspect ratios were found to be in good agreement with the creeping flow predictions for cavity Reynolds numbers $Re < 50$ and aspect ratios $a < 1$. The structure of the flow in this geometry was found to be similar to that in closed cavities of the same shape. The position and strength of the principal vortex were observed to be nearly independent of the existence of a free surface, and the gas-liquid interface was found to significantly stabilize the rotational motion in shallow cavities.

Eduardo L. Canedo
Costel D. Denson
Department of Chemical Engineering
University of Delaware
Newark, DE 19716

Introduction

Rolling pools of viscous liquids are frequently encountered in industrial equipment used for the processing of polymer melts. Devolatilization and gas absorption operations, for example, are conducted in screw extruders under conditions where liquid is contained in a partially filled channel and a rolling pool of liquid having a free surface is formed on the pushing side of the flight. The engineering analysis of heat and mass transport processes in these and similar geometries, where rolling pools of liquid are generated, requires a fundamental understanding of the governing fluid mechanics. Until now, however, no such studies have been undertaken and the rational design of some of the more complex polymer processing operations has been difficult to effect.

This paper presents an analysis and experimental verification of the slow viscous flow in a driven cavity with a free surface next to a moving wall. The particular system that was chosen for study was the flow of a Newtonian liquid in a box-cylinder system in which the wall moves either in the direction of gravity or at right angles to it. Flow in this system is closely related to that which occurs in partially filled channels in screw extruders and wiped film geometries of similar design. Numerical procedures were required to obtain exact solutions to the equations of motion for two-dimensional creeping flow in cavities having finite aspect ratios. But, for infinitely deep cavities of finite width (semiconstrained cavities) analytic solutions could be obtained and these were found to closely agree with the exact solution for aspect ratios $a > 1$. For unconstrained cavities (infinitely wide and infinitely deep cavities) the analytic solution was found to reduce to the Moffatt (1964) result in terms of its prediction of the interfacial velocity at the line of contact with the moving wall.

An important result of this work is that flow in the liquid at the gas-liquid interface is an extensional flow in which the surface velocity varies with distance from the moving wall. This means that any analysis of mass transport from rolling pools should account for extensional flow at the surface, and its enhancement of mass transfer rates. All previous work has used penetration theory and the Moffatt result of a constant velocity at the interface to compute an exposure time and rates of mass transfer. The results of the present study are expected to establish new directions in terms of the correct analysis of mass transfer from rolling pools in polymer processing equipment.

Correspondence concerning this paper should be addressed to C. D. Denson.
The present address of E. L. Canedo is Farrel Corporation, Ansonia, CT 06401.

Background

Recirculating flow in a cavity is present in a variety of applied systems other than in the channels of screw extruders, and its qualitative features have been observed and described for quite some time. Experimental and theoretical studies have been conducted in cavities of regular shape, usually rectangular, in which flow is driven by different kinds of natural or forced external

motions. The two-dimensional system most commonly studied has consisted of a closed rectangular cavity driven by a moving wall. Its geometry is completely described by the shape factor or aspect ratio, $a = A/H$, and its dynamic behavior by a Reynolds number based on the velocity of the moving wall U_o and the cavity thickness H, as represented in Figure 1. For a square cavity ($a = 1$) at high Reynolds number ($Re \to \infty$) the flow field consists of a single steady, essentially inviscid vortex surrounded by a thin boundary layer. This model was proposed simultaneously by Squire (1956) and by Batchelor (1956), who presents a complete analysis of the case. In the other extreme, at low Reynolds number ($Re \to 0$), the creeping motion of the liquid has generated less interest.

Burggraf (1966) presented a detailed study of the fluid mechanics of a separate plane vortex and developed an approximate analytic solution valid for any value of the Reynolds number. The solution shows the development of the flow from a purely viscous eddy at low Re to an effectively inviscid rotational core at high Re, in agreement with Batchelor's model. The paper also includes a numerical solution for the flow in a square cavity driven by a moving wall, at $0 \leq Re \leq 400$, as well as solutions of the energy equation for several boundary conditions.

Pan and Acrivos (1967) presented a detailed numerical solution for the creeping flow ($Re = 0$) in a rectangular cavity driven by a moving wall with aspect ratios in the range $0.2 \leq a \leq 4$. The results, obtained by a finite-difference procedure applied to a very refined mesh, are probably the best in the available literature to that time for the case $Re = 0$. The solution shows the multicellular pattern of counterrotating vortices for $a = 0.5$ (two regions) and $a = 0.2$ (four regions), and a succession of square corner vortices for all values of the shape factor as predicted by Moffatt (1964). This fundamental paper also includes some experimental data taken in a water cavity with $a = 1.0$ and $a = 10$ over the range $20 \leq Re \leq 4{,}000$; the data are in fairly good agreement with the predictions of the Burggraf (1966) numerical solution.

Other experimental and theoretical studies of cavity flow include the early work of Mills (1963), Weiss and Florsheim (1965), and O'Brien (1972). Recently, Joseph and his collaborators developed a general analytical approach to slow viscous flows with and without free surfaces. The applications include cavity flow driven by different means (Sanders et al., 1980; Trogdon and Joseph, 1982).

The slow viscous flow near sharp corners was first studied by Lord Rayleigh (1911) and later by Dean and Montagnon (1949), Moffatt (1964), Lught and Schwiderski (1965), and Gupta et al. (1981). In his fundamental paper, Moffatt considered the case of gas-liquid-solid dynamic contact line. Under the assumption of a planar gas-liquid interface, the interfacial velocity is constant and given, when the entrance angle is $\pi/2$, by:

$$u_o = \frac{2}{\pi} U_o \tag{1}$$

where U_o is the speed of the moving wall.

Huh and Scriven (1971) generalized Moffatt's analysis, including the flow in the gas (or immiscible liquid) phase, and discussed the mathematical singularity at the dynamic contact line. This fact, the discontinuity of the velocity at the contact line, and the resultant infinite stresses, is characteristic of the above approach. Although some successful attempts have been made to model the flow near the dynamic contact line with a slip boundary condition (Dussan, 1976; Hocking, 1977), the question is still open and will probably remain so until a better understanding of the fluid-solid interactions at a molecular level is reached.

The Problem

We are interested in the fluid mechanics of the cavity-cylinder system. Figure 1 shows its basic geometrical features. In particular, we are interested in the recirculating flow generated in the liquid inside the box by the motion of the cylinder. Since the main attributes of this flow are the constrained geometry and the presence of a gas-liquid interface, the principal characteristic length is H, the distance between the moving cylinder and the fixed back wall. If $H \ll R$, the curvature of the moving wall can be neglected. Figure 2 shows the simplified geometry and sets the nomenclature.

We will assume that the liquid behaves as a Newtonian incompressible fluid and that isothermal conditions prevail: liquid density, ρ, and viscosity, η, are constants. The gas above the liquid remains at a uniform constant pressure p_o, and its viscosity is negligible compared with the liquid viscosity. We will also assume that the cylinder rotates at a slow, constant angular

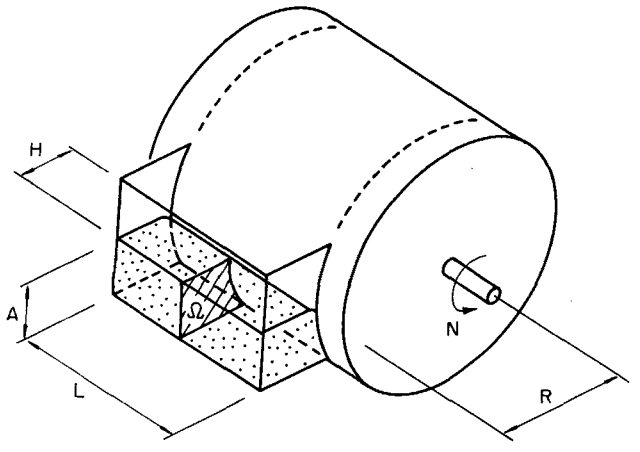

Figure 1. Cavity-cylinder system showing principal geometric parameters and region of interest Ω.

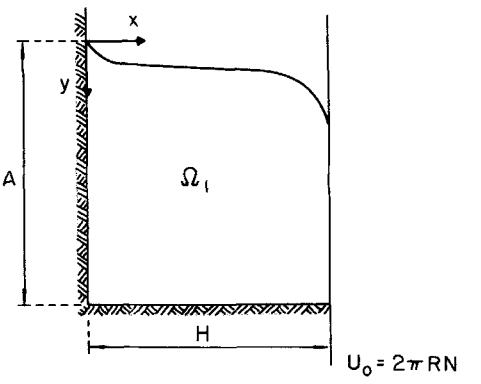

Figure 2. Simplified flow domain Ω_1 and notation.

speed N, and will consider the steady, fully developed motion generated in the liquid. Moreover, we will neglect the influence of the thin lubrication film that flows from the cavity at the bottom and reenters at the dynamic contact line.

To further simplify the problem, two more approximations will be made. First, we will consider only the creeping motion of the liquid, in the limit $Re \to 0$. This approximation is quite reasonable for the present work since the main interest is in relatively slow flows of highly viscous liquids. Second, we will assume a planar gas-liquid interface. This assumption is more serious. It is certainly not valid near the corners. However, it may be more reasonable for the central part of the gas-liquid interface.

Under these circumstances, the equations of motion can be reduced to:

$$\nabla^4 \psi = 0 \tag{2}$$

in $\Omega_1^* = [(x^*, y^*)/0 < x^* < 1, 0 < y^* < a]$, where $\psi = \psi(x^*, y^*)$ is the dimensionless stream function defined by

$$u^* = \frac{u}{U_0} = -\frac{\partial \psi}{\partial y^*}$$

$$v^* = \frac{v}{U_0} = \frac{\partial \psi}{\partial x^*} \tag{3}$$

u^* and v^* are the x^* and y^* components of the dimensionless velocity vector, respectively.

Boundary conditions for Eq. 2 are:

$$\frac{\partial \psi}{\partial x^*} = 0 \qquad x^* = 0, 0 < y^* < a \tag{4}$$

$$\frac{\partial \psi}{\partial y^*} = 0 \qquad y^* = a, 0 < x^* < 1 \tag{5}$$

$$\frac{\partial \psi}{\partial x^*} = 1 \qquad x^* = 1, 0 < y^* < a \tag{6}$$

$$\frac{\partial^2 \psi}{\partial y^{*2}} = 0 \qquad y^* = 0, 0 < x^* < 1 \tag{7}$$

In addition, since the flow field is closed, we shall take $\psi = 0$ at all four boundaries.

Equation 7 expresses the vanishing shear stress at the gas-liquid interface. Since the shape of the "free" surface is fixed and assumed to be flat, normal stresses are unbalanced at $y^* = 0$. Figure 3 shows the boundary value problem.

Analytic Solution for $a \to \infty$

No published analytic solution has been found for the problem just described, or for one that is closely related. The main difficulty can be traced to the constrained field. Moffatt (1964) demonstrated that the completely unconstrained problem ($A \to \infty$, $H \to \infty$) has a simple similar solution. Here we will present an analytic solution for the partially constrained problem ($A \to \infty$), which we expect will represent fairly well the flow near the gas-liquid interface for deep boxes, $a \gg 1$.

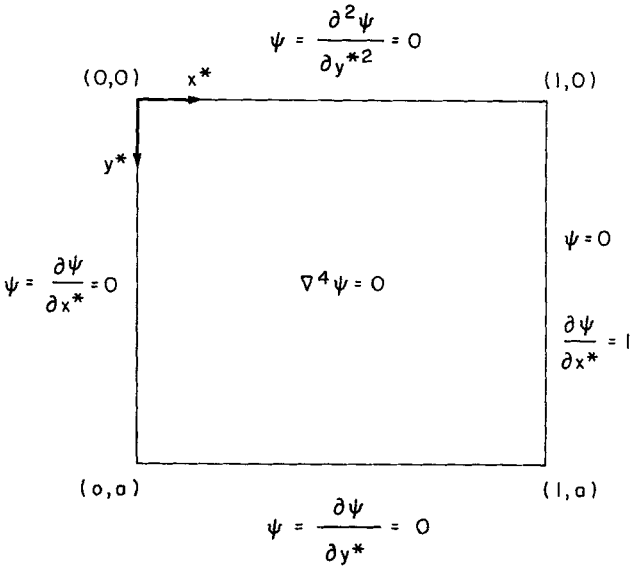

Figure 3. Boundary-value problem in domain Ω_1^*.

Under these circumstances, the problem reduces to Eq. 2 in $\Omega_2^* = [(x^*, y^*)/0 < x^* < 1, y^* > 0]$ with boundary condition Eqs. 4, 6, and 7. Equation 5 is now replaced by the regularity condition:

$$|\psi| < \infty \qquad y^* \to \infty, 0 < x^* < 1 \tag{8}$$

Equation 2, along with boundary condition Eqs. 4 and 6 with $\psi = 0$, and Eqs. 7 and 8, admit the separable solution in Ω_2^*.

$$\psi_\lambda = C\left[\left(1 + \frac{\lambda \cosh \lambda - \sinh \lambda}{\sinh \lambda} x^*\right) \cdot \sinh \lambda x^* - \lambda x^* \cosh \lambda x^*\right] \cdot \sin \lambda y^* \tag{9}$$

where C is an arbitrary constant and λ is a parameter, $0 < \lambda < \infty$. We seek a solution of the complete boundary value problem of the form

$$\psi = \int_0^\infty \psi_\lambda \, d\lambda \tag{10}$$

(See Battacharji and Savic, 1965, for a related problem in cylindrical coordinates.) Application of the remaining boundary condition, Eq. 6 with $\partial \psi / \partial x^* = 1$, results in

$$C = \frac{2}{\pi} \cdot \frac{\sinh \lambda}{\sinh^2 \lambda - \lambda^2} \tag{11}$$

and the solution of the problem is finally:

$$\psi = -\frac{2}{\pi} \int_0^\infty F(x^*, \lambda) \frac{\sin \lambda y^*}{\lambda} \, d\lambda \tag{12}$$

with

$$F = \frac{(1 - x^*) \sinh \lambda \sinh \lambda x^* - \lambda x^* \sinh \lambda (1 - x^*)}{\sinh^2 \lambda - \lambda^2} \tag{13}$$

At large distances from the gas-liquid interface, the problem resembles Couette flow between parallel plates with zero net flow rate. For $y^* > 0$, we can change variables in Eq. 12 by defining $\xi = \lambda y^*$:

$$\psi = \frac{2}{\pi}\int_0^\infty F\left(x^*, \frac{\xi}{y^*}\right)\frac{\sin\xi}{\xi}\,d\xi \tag{14}$$

And then, as $y^* \to \infty$ we have

$$\psi_\infty = \lim_{y^*\to\infty}\psi(x^*, y^*) = -\frac{2}{\pi}F_o(x^*)\int_0^\infty \frac{\sin\xi}{\xi}\,d\xi \tag{15}$$

where

$$F_o = \lim_{y^*\to\infty} F\left(x^*, \frac{\xi}{y^*}\right) = \lim_{\lambda\to 0} F(x^*, \lambda) = x^{*2}(1 - x^*) \tag{16}$$

Thus,

$$u_\infty^* = -\frac{\partial\psi_\infty}{\partial y^*} = 0 \tag{17a}$$

$$v_\infty^* = -\frac{\partial\psi_\infty}{\partial x^*} = x^*(3x^* - 2) \tag{17b}$$

which is the expected result for plane Couette flow with zero net flow.

The motion represented by Eq. 12 can be considered as a recirculating vortex around a point at infinity. The stream function reaches its minimum at this point and, from the definition of y, it is clear that the center of the vortex is a stagnant point: $u_1^* = v_1^* = 0$. From Eq. 17, the position of the center is

$$(x_1^*)_\infty = \frac{2}{3}$$

$$(y_1^*)_\infty = \infty \tag{18}$$

The value of the stream function at its center can be found by substituting these values into Eq. 15:

$$(\psi_1)_\infty = -\frac{4}{27} = -0.14815 \tag{19}$$

The velocity profile at the gas-liquid interface is given by

$$u_o^* = -\left.\frac{\partial\psi}{\partial y^*}\right|_{y^*=0} = \frac{2}{\pi}\int_0^\infty F(x^*, \lambda)\,d\lambda \tag{20}$$

Where $F(x^*, \lambda)$ is defined in Eq. 13.

The integral in Eq. 20 was evaluated using a combination of analytical and numerical procedures (Canedo, 1985). The results are shown in Figure 5 as the curve labeled $a = \infty$.

Along the gas-liquid interface, the flow is purely extensional. The normal stress distribution at the interface can be computed

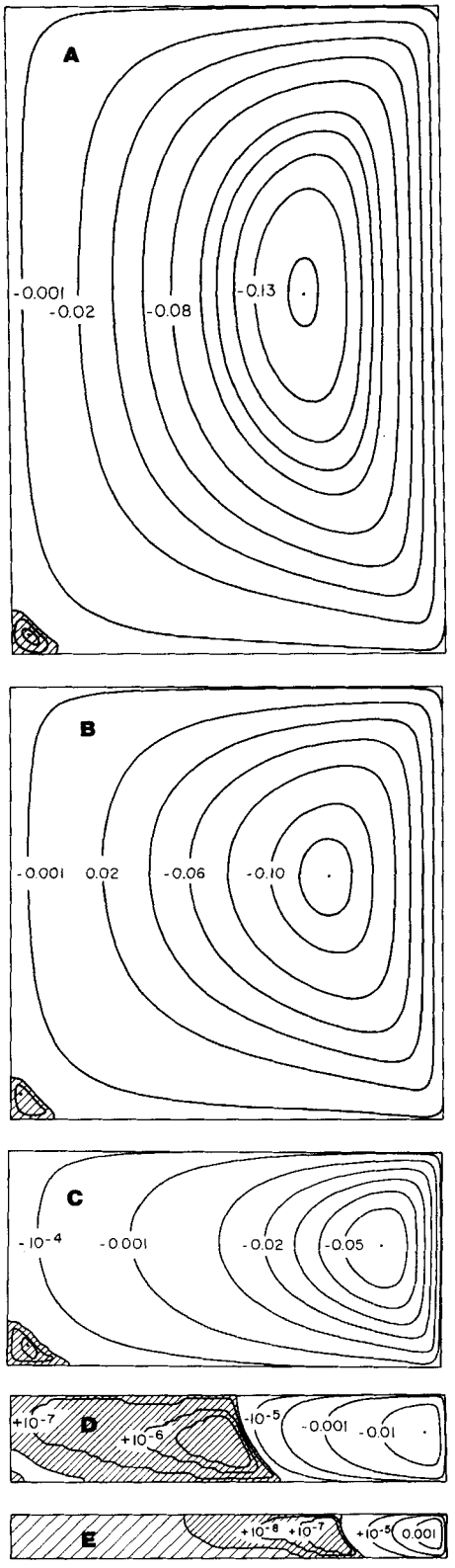

Figure 4. Streamline pattern in cavity for several values of aspect ratio according to numerical solution of Eqs. 22.

(a) $a = 1.5$; (b) $a = 1.0$; (c) $a = 0.5$; (d) $a = 0.2$; (e) $a = 0.1$.
Orientation the same as in Figure 2, with gas-liquid interface at top and moving wall at right side
Numbers near streamlines are values of stream function
Regions of counterrotating motion are fine shaded

by direct numerical differentiation of the previous results:

$$\epsilon_o = \epsilon(x^*, o) = 2\frac{du_o^*}{dx^*} \tag{21}$$

Figure 6 shows the computed results.

Numerical Solution

The analytic solution developed in the last section does not take into account one of the main features of the problems under study: the recirculating nature of the flow with closed streamlines. No simple analytic approach to confined recirculating flows has been found. In the available literature, nonslip boundary conditions are always used: the velocity at the borders (or, in the stream function formulation, ψ and its first normal derivative at the borders) are given. In the present case, the use of a free-surface boundary condition (the second normal derivative of the stream function vanishes at one border) is a nontrivial extension of the classical cavity flow problem.

To simplify the numerical solution, the fourth-order biharmonic equation, Eq. 2, is replaced by an equivalent system of two second-order equations. Introducing the auxiliary variable ω results in:

$$\Delta^2\psi = \omega \tag{22a}$$

$$\Delta^2\omega = o \tag{22b}$$

This substitution allows the use of faster and better known methods developed for these classical second-order equations known as the Poisson equation and the Laplace equation, respectively. In the present case the auxiliary variable ω can be recognized as the dimensionless vorticity distribution, which is defined by:

$$\omega = \frac{\partial v^*}{\partial x^*} - \frac{\partial u^*}{\partial y^*} \tag{23}$$

Upon discretization, Eqs. 22 were solved by a double iterative technique proposed by Greenspan and Schultz (1972). A square mesh of size h in the range $0.01 \leq h \leq 0.05$ was used.

Computations were performed for several values of a, the aspect ratio of the box. Contour plots of the stream function (streamlines) are given in Figure 4 for $a = 1.5$, 1.0, 0.5, 0.2, and 0.1. The first three cases show the main recirculating flow and a small counterrotating vortex at the corner between the two fixed walls. At $a = 0.2$, the countercirculating region extends to the gas-liquid interface, and both tertiary and quaternary corner vortices are shown. Numerical computations not plotted here reveal that the secondary motion extends to the surface at about $a = 0.25$. At $a = 0.1$, several vortices of opposite direction fill the box.

The motion outside the principal vortex is extremely slow. The stream function range in these regions is typically 10^{-9} to 10^{-6}, and the maximum dimensionless velocity is of the order of 10^{-6}. Thus, for many practical purposes, the fluid could be considered stagnant. The grid used was fine enough (the mesh size parameter h was taken between 0.025 and 0.010) to detect the secondary motion. However, the error condition required to obtain convergence of the numerical procedure near the dynamic contact line prevented an accurate quantitative description of the internal structure in this region.

Table 1. Parameters for the First Two Vortices for Various Aspect Ratios

	First Vortex (Main)			Second Vortex		
a	ψ_1	x_1^*	y_1^{**}	ψ_2	x_2^*	y_2^{**}
1.5	−0.1414	0.68	0.44	+8.5 · 10-6	0.042	0.972
1.0	−0.1138	0.74	0.44	+4.9 · 10-6	0.04	0.96
0.5	−0.0589	0.86	0.44	+0.8 · 10-6	0.05	0.92
0.2	−0.0233	0.95	0.44	+4.4 · 10-6	0.49	0.57
0.1	−0.0114	0.97	0.49	+1.7 · 10-6	0.74	0.52

Table 1 shows the value of the stream function at the center of the first and second vortices in all cases. This value of the stream function is the strength of the vortex and is equal to the flow rate per unit length. The position of the center is given in terms of a stretched vertical coordinate y^{**},

$$y^{**} = \frac{y^*}{a} = \frac{y}{A}$$

The flow near the moving wall in a cavity with a free surface does not differ greatly from the flow near the moving wall in a closed cavity. The center and strength of the principal vortices are nearly identical in both cases, although minor differences do exist. Away from the moving wall, however, the free surface has a marked stabilizing effect on the recirculating motion as compared with the case where no free surface exists. This effect can be appreciated by noting the position of the secondary vortex for $a = 0.5$ and the absence of corner vortices in the free surface-fixed wall vertex. In this work $x_2^* = 0.05$, while for a closed cavity x_2^* is found to have a value of $x_2^* = 0.21$ (Pan and Acrivos, 1967). The influence on the gas-liquid interface becomes more pronounced as the box becomes wider and shallower. Figure 4 shows clearly the increasing asymmetry of the flow field as the box aspect ratio decreases, while in a cavity without free surface, the creeping flow pattern is perfectly symmetric about a line $y^{**} = 0.5$ in all cases (Pan and Acrivos, 1967).

Figure 5 shows the interfacial velocity profile for several values of the parameter a; the analytic solution ($a \to \infty$) is also represented for comparison. For deep, narrow boxes, $a > 1$, the analytic solution is an excellent approximation. In fact, for $a > 5$, the analytic solution could not be distinguished from the numerical results over most of the field.

Near the moving wall the numerical results show a maximum and then decrease to zero at the dynamic contact line, $x^* = 1$, in contrast with the discontinuity of the analytic solution at this point. Table 2 gives the maximum interfacial speed and its position, values that were obtained by quadratic interpolation.

For shallow, wide boxes the fluid can be considered stagnant over most of the interface. The significant motion is reduced to a small zone near the dynamic contact line. As a measure of the extension of the stagnant region, we can take the point x_o^* at which the velocity reaches 1% of its maximum value:

$$u_o^*(x_o^*) = 0.01 \cdot (u_o^*)_{\max} \tag{24}$$

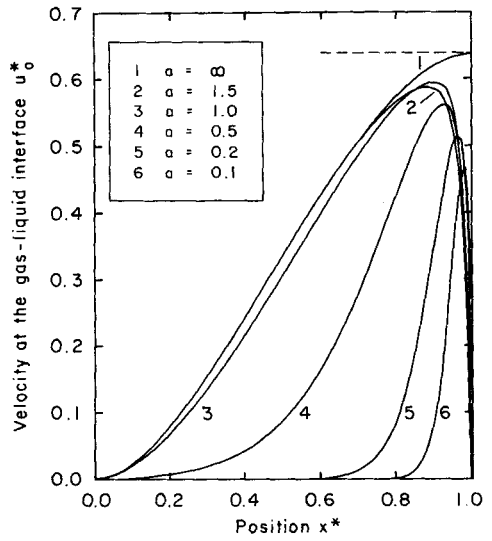

Figure 5. Interfacial velocity profiles for several values of aspect ratio according to numerical solution of Eqs. 22.

Curve 1 is result of analytic solution, Eq. 20, $a = \infty$
---- Moffatt solution

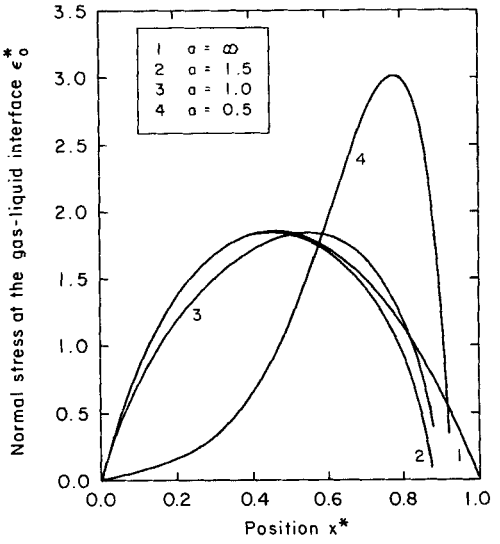

Figure 6. Normal stress distributions at gas-liquid interface for several values of aspect ratio according to numerical solution of Eqs. 22.

Curve 1 is result of analytic solution, Eq. 21, $a = \infty$.

The data can be represented to a good approximation by the expression:

$$x_o^* = 1 - 0.7 \cdot a, \qquad a \leq 0.5 \tag{25a}$$

$$x_o^* = 0.06, \qquad a \geq 0.75 \tag{25b}$$

Thus, for shallow boxes ($a < 0.5$), the extension of the "live" region is proportional to the geometric parameter a.

Figure 6 shows the dimensionless normal stress at the gas-liquid interface for several values of the parameter a. Again, for $a = 1.5$, the results of the numerical solution agree with the analytic solution ($a \rightarrow \infty$) over most of the field. The numerical solution, however, shows a discontinuity at the dynamic contact line for all values of a. For shallow boxes, a steep maximum develops near the moving wall, suggesting a strong singularity at $x^* = 1$, as $a \rightarrow 0$.

Experimental Method

A cylinder-cavity system was designed and constructed in order to conduct the experimental study. The basic apparatus consisted of a large metallic cylinder, driven by a variable speed motor, and a clear plastic box attached to it. The box was filled with a viscous liquid and the cylinder was rotated at a controlled speed. The box, which remained stationary, was held in place by a small mount that forced it against the cylinder. The system permits visual observation and photographic recording of the dynamic behavior of the liquid inside the box, Figure 1.

A stainless steel cylinder of 200 mm dia. and 155 mm length was used in combination with several Plexiglas boxes of length $L = 100$ mm with different thicknesses H, ranging from 6.5 to 62.3 mm. The drive permitted operating the cylinder at rotational speeds between about 1 and 160 rpm.

Two kinds of liquids were used in the present study: glycerol-water mixtures and polybutene 24-kerosene mixtures. Table 3 presents a summary of the significant physical properties of the liquids used in the present study: density, ρ, viscosity, η, and surface tension, σ.

The shape of the gas-liquid interface and the streamline pattern of the flow inside the cavity were visually observed and photographically recorded in a variety of experimental conditions. Interfacial velocities were measured when the box was mounted in the vertical position (on the side of the cylinder), but no velocity measurements were made when the box was mounted horizontally (on top of the cylinder).

Table 2. Maximum Interfacial Velocity and Its Location for Various Aspect Ratios

a	x^*max	(u_o^*)max
∞	1.00	0.6366
1.5	0.88	0.5886
1.0	0.90	0.5949
0.5	0.92	0.5330
0.2	0.96	0.5197
0.1	0.98	0.4791

Table 3. Physical Properties of Liquids Used in This Study at 20°C

Liquid	Conc.* %	ρ kg/m^3 $\times 10^3$	η Pa · s	σ N/m $\times 10^{-3}$
Glycerol-water	80–100	1.21–1.26	0.05–1.3	62–66
Polybutene 24-kerosene	50–100	0.85–0.90	0.06–40	32–35
Polybutene 32	100	0.90	120	35
Polybutene 122	100	0.90	650	35

*Concentration of glycerol or polybutene.

The principal independent variables can be reduced to three types:

1. Geometry of the system (dimensions and orientation of the box, amount of liquid inside the box)
2. Composition of the liquid (its physical properties: density, viscosity, and surface tension)
3. Angular speed of the cylinder

The tangential speed U_o, measured in mm/s, is related to the angular speed, measured in rpm, through the expression:

$$U_o = \frac{2\pi RN}{60} = 0.10472RN \tag{29}$$

where R is the radius of the cylinder in mm. Other operating variables, such as the state of the surface of the cylinder (roughness is one of its components) or the pressure imposed on the box when in contact with the cylinder, were difficult to control or measure. Although care was taken to maintain reproducible conditions, the effect of these variables on the flow field is difficult to ascertain. Temperature control was also a problem since the viscous heating in the gap between the box and the cylinder contributes to increasing the temperature of liquid.

The procedure in a typical experiment was as follows:

1. The box and cylinder were thoroughly cleaned with water or with cyclohexane, depending on the liquid used before, and the system was assembled in either the vertical or horizontal position.
2. A measured amount of liquid was poured into the box and its temperature was measured and recorded. The geometric ratio $a = A/H_0$ (the box aspect ratio or shape factor when in vertical position) was used as a measure of the liquid content.
3. The motor was started at some low speed (about 1 rpm), the box-cylinder alignment was checked, and the tension of the box against the cylinder was adjusted. When the box was mounted in the horizontal position, steps 2 and 3 were carried out simultaneously since the box can retain the liquid only when the cylinder is in motion.
3. The speed was increased in small steps, usually 1–2 rpm, and the flow field was observed and photographed from several angles. The temperature of the liquid was measured and recorded at the end of the experiment.

The shape of the interface and the streamline pattern were studied mostly from a lateral viewpoint. In order to show the streamlines in the liquid pool, small air bubbles were used as tracers. These bubbles were entrained by running the cylinder at a high speed for a short period of time. The speed was then reduced and the actual experiment conducted. When pictures were taken in these conditions, long exposure times were utilized to blur the small air bubbles in motion. The box was illuminated normally to the viewing direction to show the bright traces of the bubbles against a dark background. The camera was focused in the bulk liquid close to the centerline in an attempt to avoid any flow "end effect."

The interfacial velocity was measured photographically with the box mounted in the vertical position using a solid particle tracer. A small alumina pellet, approximately 1 mm in diameter, was deposited on the air-liquid interface near the back wall. The particle, which floated on the liquid surface, moved toward the cylinder. This motion was recorded with a motorized camera from a direction perpendicular to the liquid surface. The camera

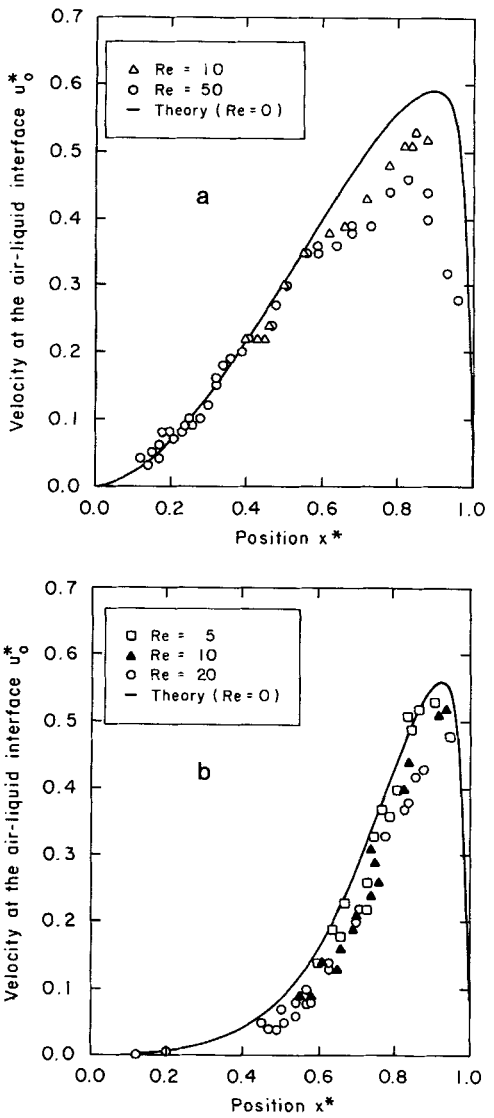

Figure 7. Interfacial velocity profile measured in box mounted in vertical position.

Glycerol-water solutions at 21°C and several cylinder speeds
——— prediction of numerical solution of Eq. 22a
(a) $a = 1.0$; (b) $a = 0.5$

was carefully focused on the interface and a series of 10 to 30 frames was exposed in each run at a rate of 3 frames per second, using a short exposure time (4 ms). The motor drive of the camera was calibrated against a mechanical chronometer before or after each session; it showed a remarkably constant time interval between frames of 0.300 ± 0.005 s. The distance between the successive positions of the particle was measured on the negatives projected at 10× magnification and the interfacial speed computed.

Results and Discussion

Measured values of the interfacial velocities for glycerol-water solutions at several cylinder speeds and two values of the aspect ratio a are shown in graphical form in Figure 7. These

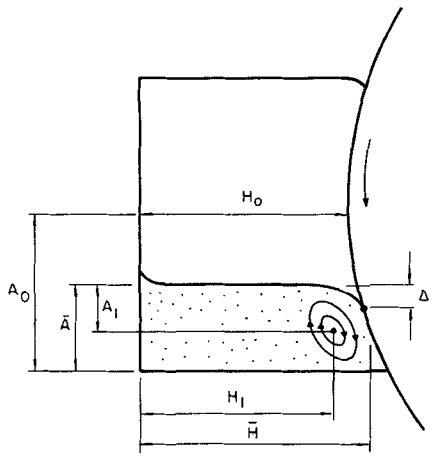

Figure 8. Definition of some geometrical parameters used in quantitative description of flow pattern inside box mounted in vertical position.

Δ, dynamic displacement depth
Position of center of principal vortex: $\bar{x}_1^* = H_1/\bar{H}$, $\bar{y}_1^{**} = A_1/\bar{A}$.

results, obtained in the range $5 \leq Re \leq 50$, were found to be in good agreement with the numerical solutions for $Re \rightarrow 0$. As described earlier, the experimental method for obtaining these velocities involved photographing tracer particles at the surface, which gives just the horizontal component of the interfacial velocity. However, this should not introduce large errors since the interfacial velocity has a significant vertical component only near the dynamic contact line. The estimated error in the horizontal velocity is less than ± 0.5 mm/s and is limited by particle size.

Experimentally determined values for the location of the center of the principle vortex are reported in terms of the variables, Figure 8,

$$\bar{x}_1^* = \frac{H_1}{\bar{H}}, \qquad \bar{y}_1^{**} = \frac{A_1}{\bar{A}}$$

Table 4, which reports these results, reflects the average of at least five different runs in each case with an average deviation of ± 0.02. It is especially to be noted that the experimental measurements at low Re show a small but significant displacement of the center of the main vortex with respect to the theoretical predictions of the numerical solution $Re \rightarrow 0$. Experimental and theoretical studies in driven cavities without a free surface exhibit a similar displacement of the center of the main vortex at finite Reynolds numbers.

Table 4. Values for Location of Center of Principal Vortex

	Theory		Exp.			
			$Re = 0.1$–0.5†		$Re = 10$–50‡	
a	$\bar{x}_1^*$	$\bar{y}_1^*$	$\bar{x}_1^*$	$\bar{y}_1^*$	$\bar{x}_1^*$	$\bar{y}_1^{**}$
0.5	0.86	0.44	0.86	0.51	0.86	0.59
1.01	0.74	0.44	0.75	0.50	0.77	0.51

†90% polybutene 24-kerosene at 21°C.
‡95% glycerol-water at 21°C

Table 5. Effect of Free Surface on Strength of Principal Vortex (ψ_{CENTER})

	ψ		
a	Open Cavity This Work	Closed Cavity Pan & Acrivos (1967)	Increase %
1.5	−0.1414	−0.13*	9
1.0	−0.1138	−0.10	13
0.5	−0.0589	−0.05	18
0.2	−0.0233	−0.02	17
0.1	−0.0114	−0.02	14

*Interpolated.

A comparison of the results obtained from the numerical solution of the present work with those of a similar investigation in closed cavities (Pan and Acrivos, 1967) shows that the presence of a free surface increases the strength and flow domain of the principal vortex, Tables 5 and 6. Note the large increase in the fraction of the cavity occupied by the principal vortex in shallow cavities ($a < 1$), reflecting the stabilization of this motion by the free surface.

When the box was mounted in the vertical position (on the side of the cylinder), the air-liquid interface appeared flat and almost horizontal in most of its extension regardless of the conditions. Appreciable curvature was found only at very high speeds, to which the collapse of the dynamic contact line invalidates the models developed in the previous sections. The air entrainment phenomena associated with this collapse are discussed elsewhere (Canedo and Denson, 1988).

At moderately low speeds a small deviation from flatness was apparent near the fixed wall (quasi-static meniscus) and near the moving wall. To obtain a simple quantitative description of the flow field in these conditions geometric characteristics were measured: the shape of the air-liquid interface near the dynamic contact line and the position of the center of the principal vortex.

A rough but useful characterization of the interfacial shape in the neighborhood of the dynamic contact line is its deviation from flatness as measured by the displacement depth Δ shown in Figure 8. Δ was measured on the projected image of the negatives at about 10× magnification. Since the photographs were taken through the lateral wall of the box, the masking effect of the quasi-static meniscus on the lateral wall causes a relatively large uncertainty in the value of the geometrical parameter Δ. The dynamic displacement depth was found to be nearly independent of the operating conditions and only varied from 3.0 to 4.6 mm for subcritical speeds for boxes mounted vertically. These results are in good agreement with the careful measurements of Δ conducted in a tape-pool system by Burley and Kennedy (1976) and Burley and Jolly (1982), as shown in Table 7.

Table 6. Effect of Free Surface on Fraction of Flow Domain Occupied by Principal Vortex

a	Open Cavity This Work	Closed Cavity Pan & Acrivos (1967)	Increase %
1.0	0.995	0.995	0
0.5	0.985	0.677	45
0.2	0.438	0.271	68

Table 7. Dynamic Penetration Depth

	This Work	Burley et al. (1976, 1982)
η, Pa · s	0.005–12	0.001–1
σ, mN/m	30–65	25–65
Δ, mm	3.0–4.6	1.0–4.0

A few experimental runs were conducted in circumstances when the box was mounted horizontally. The flow shown in Figure 9 is typical of that which develops when the gravitational field and the moving surface are at right angles to each other. In this photograph the rotating cylinder is at the bottom of the photograph and moves from left to right. Figure 10 shows how the liquid profile changes shape with changes in the velocity of the moving surface. No attempt was made to compute the shape of the interface, or the location of the center of the vortex, from first principles.

Conclusions

The structure of the flow in vertically oriented driven cavities with a free surface is not unlike that in closed cavities of the same shape. The flow field is composed of a series of progressively smaller and weaker countercirculating vortices, following the general pattern shown by Pan and Acrivos (1967). The position and strength of the principal vortex is nearly independent of the existence of a free surface, but the gas-liquid interface significantly stabilizes the rotational motion in shallow cavities.

The numerical solution of the creeping flow equations of motion presented here predicts with good approximation the interfacial velocity profile in a box-cylinder system for $Re \leq 50$. Moreover, the analytic solution developed for infinitely deep cavities, Eqs. 12–13, can be used as an excellent approximation for the flow near the gas-liquid interface in finite cavities with an aspect ratio $a \geq 1$. In this regard, the results of the present work are a significant improvement over models for flow in constrained cavities that use Moffatt's (1964) result for unconstrained systems, Eq. 1.

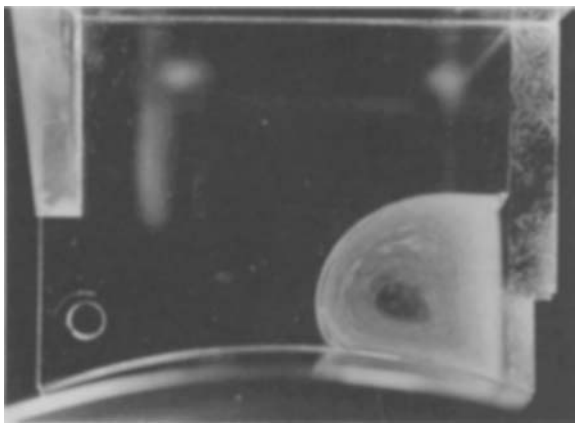

Figure 9. Typical flow pattern.
90% polybutene 24-kerosene solution (η = 5.8 Pa · s)
Box mounted horizontally, gravitational force at right angles to moving wall
Equivalent $a \approx 0.25$, U_o = 280 mm/s
Critical speed for air entrainment, about 55 mm/s

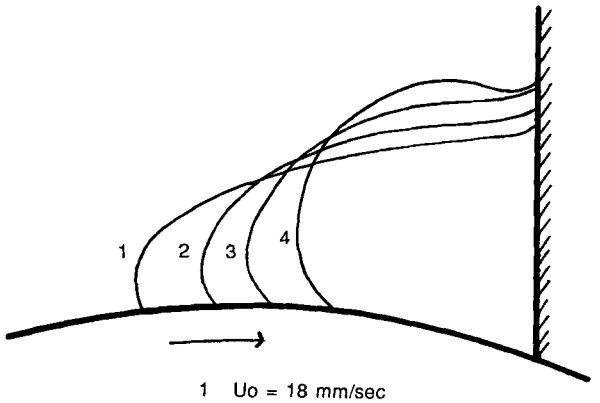

1 Uo = 18 mm/sec
2 Uo = 40 mm/sec
3 Uo = 100 mm/sec
4 Uo = 460 mm/sec

Figure 10. Influence of velocity of moving wall on shape of gas-liquid interface.
All conditions as in Figure 9 except wall speed

This investigation provides a first approximation model for the fluid mechanics of rolling pools of viscous liquids and may be useful as a basis for the analysis of heat and mass transfer processes in these systems.

Acknowledgment

This work was generously supported by the Department of Chemical Engineering at the University of Delaware and by the Werner-Pfleiderer Corporation of Ramsay, NJ. The authors also wish to acknowledge the many helpful suggestions made by M. M. Denn in the early stages of this work.

Notation

a = aspect of ratio of cavity, A/H
A = characteristic length along y axis, depth of cavity
F = function, Eq. 13
H = characteristic length along x axis, width of cavity
H_o = width of cavity at narrowed point
L = characteristic length of cavity normal to x-$y$plane
N = rotational speed of cylinder, rpm
Re = Reynolds number, $HU_o\rho/\eta$
R = radius of cylinder
u = velocity in liquid in x direction
u^* = dimensionless velocity, u/U_o
U_o = linear speed of moving wall
v = velocity in liquid in y direction
v^* = dimensionless velocity, v/U_o
x = coordinate normal to moving wall
x^* = dimensionless distance, x/H
y = coordinate parallel to moving wall
y^* = dimensionless distance, y/H
y^{**} = dimensionless distance, y/A

Greek letters

Δ = dynamic displacement depth
ϵ = dimensionless normal stress, Eq. 21
η = viscosity
λ = parameter, Eq. 9
ρ = density
σ = surface tension
ψ = dimensionless stream function, Eq. 3
ω = dimensionless vorticity function, Eq. 23

Subscripts

o = surface of liquid at gas-liquid interface
∞ = infinitely deep cavity

Literature Cited

Batchelor, G. K., "On Steady Laminar Flow with Closed Streamlines at Large Reynolds Number," *J. Fluid Mech.*, **1,** 177 (1956).

Bhattacharji, S., and P. Savic, "Real and Apparent non-Newtonian Behavior in Viscous Pipe Flow of Suspensions Driven by a Fluid Piston," *Proc. 1965 Heat Trans. Fluid Mech. Inst.*, 248 (1965).

Burggraf, O. R., "Analytical and Numerical Studies of the Structure of Steady Separated Flows," *J. Fluid Mech.*, **24,** 113 (1966).

Burley, R., and R. P. S. Jolly, "Fluid Behavior and Air Entrainment at a Three-Phase Function," Paper 46B, *AIChE Winter Nat. Meet.*, Orlando, FL (1982).

Burley, R., and B. S. Kennedy, "An Experimental Study of Air Entrainment at a Solid/Liquid/Gas Interface," *Chem. Eng. Sci.*, **31,** 901 (1976).

Canedo, E. L., "Flow and Mass Transfer in a Driven Cavity with a Free Surface," Ph.D. Thesis, Univ. Delaware (1985).

Canedo, E. L., and C. D. Denson, "Gas Entrainment in Partially Filled Channels of Screw Extruders," AIChE Mtg., New Orleans (Mar., 1988).

Dean, W. R. and P. E. Montagnon, "On the Steady Motion of Viscous Liquid in a Corner," *Proc. Cambridge Phil. Soc.*, **45,** 389 (1949).

Dussan, E. B., "The Moving Contact Line: The Slip Boundary Condition." *J. Fluid Mech.*, **77,** 665 (1976).

Greenspan, D., and D. Schultz, "Fast Finite-Difference Solution of Biharmonic Problems," *Comm. ACM*, **15,** 347 (1972).

Gupta, M. M., R. P. Manohar, and B. Noble, "Nature of Viscous Flows Near Sharp Corners," *Comput. Fluids*, **9,** 379 (1981).

Hocking, L. M., "A Moving Fluid Interface: The Removal of the Force Singularity by a Slip Flow," *J. Fluid Mech.*, **79,** 209 (1977).

Huh, C., and L. E. Scriven, "Hydrodynamic Model of Steady Movement of a Solid/Liquid/Fluid contact line." *J. Colloid Interf. Sci.*, **35,** 85 (1971).

Lugt, H. J. and E. W. Schwiderski, "Flows Around Dihedral Angles," *Proc. Roy. Soc. (Lond.)*, **A285,** 382 (1965).

Mills, R. D., "On the Closed Motion of a Fluid in a Square Cavity," *J. Roy. Aero. Soc.*, **69,** 116, 714 (1963).

Moffatt, H. K., "Viscous and Resistive Eddies Near a Sharp Corner," *J. Fluid Mech.*, **18,** 1 (1964).

O'Brien, V., "Closed Streamlines Associated with Channel Flow Over a Cavity," *Phys. Fluids*, **15,** 1089 (1972).

Pan, F., and A. Acrivos, "Steady Flows in Rectangular Cavities," *J. Fluid Mech.*, **28,** 643 (1967).

Rayleigh, Lord (J. W. Strutt), "Hydrodynamic Notes." *Phil. Mag., 21,* 117 (1911); reprinted *Scientific Papers,* vol. 6, Dover, New York (1964).

Sanders, J., V. O'Brien, and D. D. Joseph, "Stokes Flow in a Driven Sector by Two Different Methods," *J. Appl. Mech.*, **47,** 482 (1980).

Squire, H. B., "Note on the Motion Inside a Region of Recirculation (Cavity Flow)," *J. Roy. Aero. Soc.*, **60,** 203 (1956).

Trogdon, S. A., and D. D. Joseph, "Matched Eigenfunction Expansions for Slow Flow Over a Slot," *J. Non-Newt. Fluid Mech.*, **10,** 185 (1982).

Weiss, R. F., and B. H. Florsheim, "Flow in a Cavity at Low Reynolds Number," *Phys. Fluids*, **8,** 1631 (1965).

Manuscript received July 2, 1987, and revision received July 22, 1988.